



This is the accepted manuscript made available via CHORUS. The article has been published as:

# Shear-induced segregation of particles by material density

Yi Fan and K. M. Hill

Phys. Rev. E **92**, 022211 — Published 25 August 2015

DOI: [10.1103/PhysRevE.92.022211](https://doi.org/10.1103/PhysRevE.92.022211)

# Shear-induced segregation of particles by material density

Yi Fan

*The Dow Chemical Company, Midland, MI 48667, USA*

K. M. Hill\*

*St. Anthony Falls Laboratory, Department of Civil Engineering,  
University of Minnesota, Minneapolis, MN 55414, USA*

## Abstract

Recently, shear rate gradients and associated gradients in velocity fluctuations (e.g., granular temperatures or kinetic stresses) have been shown to drive segregation of different sized particles in a manner that reverses at relatively high solids fractions ( $\langle f \rangle > 0.50$ ). Here, we investigate these effects in mixtures of particles differing in material density through computational and theoretical studies of particles sheared in a vertical chute where we vary the solid fraction from  $\langle f \rangle = 0.2$  to 0.6. We find that in sparse flows,  $\langle f \rangle = 0.2$  to 0.4, the heavier (denser) particles segregate to lower shear rates similar to the heavier (larger) particles in mixtures of particles differing only in size. However, *there is no segregation reversal* at high  $f$  in mixtures of particles differing in density. At all solids fractions, heavier (denser) particles segregate to regions of lower shear rates and lower granular temperatures, in contrast with segregation of different-sized particles at high  $f$ , where the heavier (larger) particles segregate to the region of higher shear rates. Kinetic theory predicts well the segregation for both types of systems at low  $f$  but breaks down at higher  $f$ 's. Our recently proposed mixture theory for high  $f$  granular mixtures captures the segregation trends well via the independent partitioning of kinetic and contact stresses between the two species. In light of these results, we discuss possible directions forward for a model framework that encompasses segregation effects more broadly in these systems.

PACS numbers: 47.57.Gc, 81.05.Rm

---

\* kmhill@umn.edu

## I. INTRODUCTION

Granular materials tend to segregate when particles in the mixture differ in size, material density, shape or other properties. Segregation due to differences only in material density (often called *density segregation*, e.g. Refs. [1–3]) has wide implications for a variety of natural and industrial processes. For example, in a vibrofluidized bed, density difference between an impurity and the rest of the particles in the bed creates problems for a variety of processes employing this mechanism for transport (e.g., Ref. [4]). In longitudinal bars of braided rivers, this segregation can give rise to local accumulations of economically important denser materials (e.g. gold, uranium, and diamonds) due to the separation of these minerals from particles that are less dense (e.g. sand and gravel) [5]. The implications of segregation for geomorphological issues are even broader, as evidence points to the influence of local variation of particle density on local variability of erosion rates [6] and sediment transport rates [7] compared to expected rates (e.g., Ref. [8]).

Segregation according to particle density has been studied experimentally and computationally under a variety of boundary conditions and methods of excitation including vibrated systems [2–4, 9] and sheared systems such as gravity-driven flows in rotating drums [10–15] and down inclined planes [16], and shear bands in split-bottom cells [17]. In vibrated systems, several factors have been shown to play important roles in the segregation process, including convection [1], gravity [4], interstitial air [9], and granular temperature (essentially, the kinetic energy associated with velocity variances) [1, 18]. In sheared flows, similar mechanisms have been shown to influence the segregation processes, including variations in particle concentration (e.g., Ref. [17, 19]). In this paper, we distinguish between segregation according to “particle density” (the focus of this paper) and segregation associated with variations of “concentration,” or solids fractions, by restricting our use of the words “dense” and “less dense” to refer to the material density of the particles  $\rho_m$  and use phrases such as “high/low concentrations” (or “sparse flows”) to refer to relative solid fractions  $f$ .

In sparse sheared flows, kinetic theory (e.g., [20–23]) has been used successfully to model and predict segregation in simulations [20] and experiments [24]. The segregation predictions may represent segregation according to several competing elements: gravity, granular temperature, pressure and diffusion “forces” (e.g., Refs. [20, 22, 23]). For example, gravity segregates denser particles downward (in the direction of gravity) relative to less dense

particles (e.g., Ref. [23]) while a gradient of granular temperature segregates denser particles to lower granular temperature (e.g., [20, 21]). For low-to-moderate system-averaged solid fractions ( $\langle f \rangle$  up to 0.4), kinetic theory predicts segregation trends well [25]. Kinetic theory has been shown to be similarly effective in predicting segregation by temperature gradient in mixtures of different sized particles at low-to-moderate  $f$ 's [25, 26], where the heavier (larger) particles also segregate to regions of lower temperature. However, as we detail shortly, for sufficiently high  $f$ 's, we have shown that for particles of different sizes, the segregation reverses, that is, heavier (larger) particles segregate to regions of higher shear rates and higher granular temperatures [17, 26], a phenomenon kinetic theory fails to capture. These trends at high  $f$  have not been investigated for segregation of particles differing in material density.

In most studies of sheared systems of relatively high system-averaged solid fractions  $\langle f \rangle$ , the primary focus of segregation of granular mixtures has involved the effect of gravity, while the effect of granular temperature has not been thoroughly explored. Typically, in high- $f$  flows, similar to sparse flows, denser particles sink relative to equal-sized lighter neighbors, and less dense particles rise. In high  $f$  flow, Khakhar *et al.* [10] proposed a ‘buoyancy’ mechanism, which was shown to successfully reproduce gravity-driven segregation according to particle density in rotating drums [11]. Specifically, particles lighter than the surrounding mixture of particles experience a buoyancy force greater than their weight and rise, and particles denser than the surrounding mixture sink. For example, for flow of such a mixture down an plane inclined by  $\theta$  relative to the horizontal, the segregation flux of the denser particles normal to the flow may be expressed according to:

$$f_d(v_d - v) = K[(\rho_d - \rho_l)/\rho_d]f\phi_d\phi_l. \quad (1)$$

Here,  $K = CV\rho_d g \cos\theta$  is a characteristic “segregation velocity”, where  $C$  is inversely related to resistance to local relative motion, and  $V$  is the volume of a particle.  $v_i$  is the velocity component of species  $i$  in the segregation direction, typically normal to the system-averaged flow direction.  $\rho_i$  is the material density of species  $i$ ,  $f_i$  is the local solids fraction of species  $i$ , and  $\phi_i$  is the local concentration of particles of species  $i$  ( $\phi_i = f_i/\Sigma_i f_i$ ). The subscripts  $i=d$  and  $l$  denote denser and less dense particles, respectively. For the variables associated with the mixture dynamics no subscript is used (e.g.,  $f = f_d + f_l$ ). We note one potentially confusing issue: while one would expect  $v$ , the system-averaged velocity for the segregation

direction, to be zero, there are exceptions in some practical applications of this framework. For example, in the flow of particles in a thin surficial layer in a rotating drum (an original application for Equation 1 in Ref. [10]), the particles dilate as they move through the first half of the flowing layer and then they contract through the second half. Still, the local value for  $v$  is typically taken to be the velocity in the *spatially-averaged* flow direction rather than the normal direction at each location. To account for cases such as this, for the purposes of the discussion in this paper, we keep the explicit representation in  $v$  in Equation 1 and related expressions of the segregation flux.

More recent work by Khakhar and colleagues (Refs. [13, 27, 28]) illuminated the form of the inverse drag function  $C$  by considering movement of particles differing in density through an *effective* medium and showed the drag increased with an effective temperature. While this latter work demonstrated how temperature should influence the drag coefficient, it did not address the issue of temperature as a driving force of segregation alone. When considering results from mixtures of different sized particles, one would expect temperature gradients to have the ability to segregate particles in high  $f$  systems as well.

Specially, we recently showed that gradients in granular temperature (or kinetic stress) associated with shear rate gradients can drive segregation in high- $f$  sheared mixtures of different sized particles [19, 29, 30]. Further, we showed that at relatively high solids fraction  $f$ , the segregation tendency reversed. That is, on the one hand, we found that in sparse systems large particles segregate to regions of high granular temperature and high shear rates, consistent with previous reports (e.g., Refs. [20–23, 25]). On the other hand, we found that at higher solids fractions,  $f \approx 0.5$  to  $0.6$ , the large particles segregate to regions of low granular temperature. To this point, no analogous study has been performed for mixtures of particles differing only in density. Further, one would expect the segregating effects of granular temperature gradients should compete with the ‘buoyancy effect’ in these mixtures, an important detail for predicting and possibly manipulating segregation in high- $f$  sheared flows.

In this paper, we describe our computational and theoretical efforts to understand the effects of granular temperature gradients on segregation of binary mixtures differing only in material density, particularly for high solids fractions. To isolate the effect of shear rate gradients from the effect of gravity, we present discrete element method (DEM) simulations of mixtures of particles differing only in density sheared in a vertical chute [Fig. 1(a)]. The

vertical chute is ideal for studying the effect of shear rate gradients and associated granular temperature gradients on segregation because of its simple geometry but inhomogeneous flow structure. To determine whether or not there is a segregation transition analogous to that in mixtures of particles differing only in size, we simulate mixtures over a range of solids fractions, from sparse to high solids fractions. We investigate two theories for their ability to reproduce segregation in these systems: (1) kinetic theory and (2) our mixture theory previously derived for mixtures of different sized particles [19, 29]. We show that kinetic theory is qualitatively effective at all solids fractions we investigate but breaks down quantitatively at high solids fractions. Our mixture theory, focused on effects associated with shear rate gradients, such as gradients in granular temperature and kinetic stress, adapts reasonably well to these mixtures of particles differing only in density. In present form, though, our theory lacks quantitative detail. In our discussion and conclusion sections, we point out shortcomings of this new model and describe ongoing work to improve upon the details.

## II. SIMULATION METHOD AND SETUP

For our computational simulations, we use the discrete element method (DEM) [31] with a soft sphere model so that each interparticle contact typically endures over several time steps. As is typical, we calculate the forces on each particle at each time step, and from these deduce the subsequent movements and positions of all particles throughout the simulations. We use a nonlinear interparticle contact model based on Hertzian and Mindlin contact theories [32] with damping components calculated based on experimental data (Ref. [33]). The interparticle forces  $\mathbf{F} = \mathbf{F}_n + \mathbf{F}_t$ , each has components normal ( $\mathbf{F}_n$ ) and tangential ( $\mathbf{F}_t$ ) to the plane of contact:

$$F_n = -k_n \delta_n^{3/2} - \eta_n \delta_n^{1/4} \dot{\delta}_n, \quad (2a)$$

$$F_t = \min \left\{ -k_t \delta_n^{1/2} \delta_t - \eta_t \delta_n^{1/4} \dot{\delta}_t, \mu F_n \right\}, \quad (2b)$$

In these equations,  $\delta_n$  and  $\delta_t$  denote deformations from interparticle contact as effective overlap in the directions normal and tangential to the plane of contact; throughout these equations, subscripts  $n$  and  $t$  refer to the directions normal and tangential to the plane of contact, respectively.  $\mathbf{V}_n = (d\delta_n/dt)\mathbf{n}$ , and  $\mathbf{V}_t = (d\delta_t/dt)\mathbf{t}$  are relative velocities of

TABLE I. Material properties used in DEM simulations. The less dense particles have similar properties to glass, although to reduce the computational time we reduce the Young’s modulus by a factor of  $O(10^2)$ , similar to our previous studies [29, 30]. The denser particles have the same properties except density, which is close to that of steel.

Property	less dense	dense
Material density ( $\text{kg/m}^3$ )	2520	7800
Young’s modulus (GPa)	0.1	0.1
Poisson ratio	0.22	0.22

TABLE II. Values of contact parameters used in the force model for the DEM simulations for the three possible pairs of interacting particles, as indicated in the first row.

Parameters	less dense	denser	less dense
	less dense	denser	denser
$k_n$ ( $\text{N/m}^{3/2}$ )	$1.57 \times 10^6$	$1.57 \times 10^6$	$1.57 \times 10^6$
$k_t$ ( $\text{N/m}^{3/2}$ )	$2.06 \times 10^6$	$2.06 \times 10^6$	$2.06 \times 10^6$
$\eta_n$ ( $\text{N s/m}^{5/4}$ )	$2.85 \times 10^{-1}$	$5.01 \times 10^{-1}$	$3.50 \times 10^{-1}$
$\eta_t$ ( $\text{N s/m}^{5/4}$ )	$3.26 \times 10^{-1}$	$5.74 \times 10^{-1}$	$4.01 \times 10^{-1}$
$\mu$	0.4	0.4	0.4

contacting particles.  $\mathbf{n}$  and  $\mathbf{t}$  are unit vectors in each direction.  $k_n$ ,  $k_t$ ,  $\eta_n$ , and  $\eta_t$  are interaction coefficients derived from materials properties as described in Refs. [32] and [33]. Sliding occurs according to the Coulomb law of friction when  $|\mathbf{F}_t|/|\mathbf{F}_n|$  exceeds the coefficient of friction  $\mu$ . The material properties to calculate the interaction coefficients are based on particles 2 mm in diameter with all properties similar to ‘glass’ particles, except material density: one particle density is similar to that of glass, and the other, similar to that of steel (Table I). The interaction coefficients for all contacts in the mixtures we describe in this paper are shown in Table II. For the simulations described here, we use an equal volume of the two types of spheres. Each species has a 10% polydispersity in the particle diameters to impede particle ordering.

The boundary conditions for our simulations are those of a vertical chute of dimensions

$D = 20$  mm,  $W = 50$  mm, and  $L = 50$  mm in the  $x$ -,  $y$ -, and  $z$ -directions, respectively [Fig. 1(a)]. Our chute has one pair of vertical side walls (perpendicular to the  $y$ -direction), which are roughened using 2 mm spheres in a random close-packed arrangement. The boundaries are periodic in the  $z$ - (vertical) and  $x$ - directions. We perform simulations for several different total system-averaged solid fractions from  $\langle f \rangle = 0.2$  to 0.6 by varying the total numbers of particles in the systems (from  $\approx 2500$  to 8000 particles). We denote the velocity  $\mathbf{u} = u\mathbf{x} + v\mathbf{y} + w\mathbf{z}$  according to the directions noted in Fig. 1(a).

For each simulation, the particles are initially arranged randomly in the chute and then released with small random velocities. After their initial release, particles collide with one another and with the vertical walls. Dissipation of energy through interparticle and wall-particle interactions limits the velocity throughout the cell, and a steady state velocity is reached for most of the simulations after a time between a fraction of a second and several seconds as will be discussed. Exceptions will be noted below. We monitor the segregation and other kinematics until the segregation appears to have reached steady state, and then

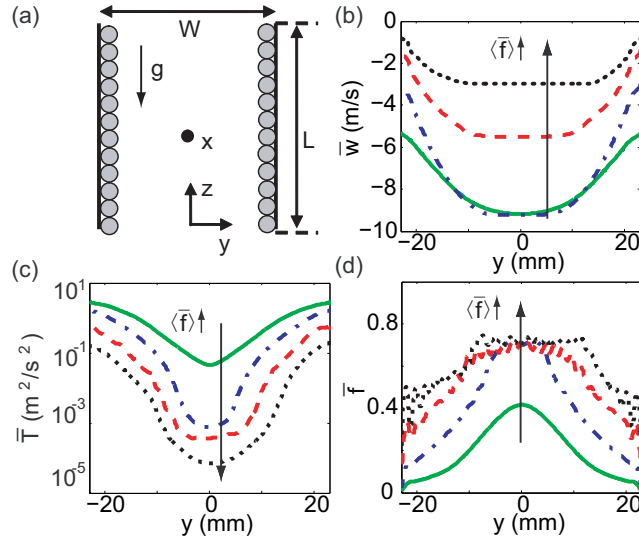


FIG. 1. (Color online) (a) Sketch of a vertical chute. (b)-(d) Time-averaged profiles of kinematic quantities for four mixtures at steady state, here  $t = 5 - 6$  s for  $\langle f \rangle = 0.2$  (green solid curve),  $t = 20 - 30$  s for  $\langle f \rangle = 0.4$  (blue dash-dotted curve),  $t = 30 - 40$  s for  $\langle f \rangle = 0.5$  (red dashed curve), and  $t = 300 - 310$  s for  $\langle f \rangle = 0.6$  (black dotted curve): (b) streamwise velocity  $\bar{w}$  of the mixture, (c) kinematic granular temperature  $\bar{T} = (\overline{u'u'} + \overline{v'v'} + \overline{w'w'})/3$  of the mixture, (d) local solid fraction of the mixture  $\bar{f}$ .



terminate the simulations (as discussed in Sec. III).

### III. SIMULATION RESULTS

The steady-state profiles of the streamwise velocity  $\overline{w}$ , the sum of the mean square velocity fluctuations (what one might call the kinematic granular temperature  $\overline{T} = (\overline{u'u'} + \overline{v'v'} + \overline{w'w'})/3$ ) and the solids fraction  $\overline{f}$  for the mixture are plotted in Figs. 1 (b)-(d). (Here and throughout we use the notation  $\overline{q}$  to denote the time average of measured quantity  $q$ . We average over the results over relatively short times in the segregation process, typically 0.5 s intervals.) We note these results are similar to those previously published for monodisperse systems (e.g. Refs. [34–36]) and for mixtures of particles differing only in size (Refs. [19, 26, 29]). At high  $\langle f \rangle$ , the velocity profile  $\overline{w}(y)$  resembles a plug flow with high shear rates at the side walls, while at the lower solid fractions, the velocity is higher and the profile is roughly parabolic [Fig. 1 (b)]. In all cases,  $\overline{T}$  is highest near the walls where the shear rate  $\dot{\gamma} = d\overline{w}/dy$  is the greatest, and increases at every point as  $\langle f \rangle$  decreases [Fig. 1 (c)]. Regions of high  $\overline{T}$  and high  $\dot{\gamma}$  (near the walls) correspond to regions of low  $\overline{f}$  [Fig. 1 (d)].

Figure 2 shows snapshots at the beginning and the end of the simulations for three representative solids fractions ( $\langle f \rangle = 0.2, 0.4$ , and  $0.6$ ). Segregation occurs in the horizontal direction under gradients of shear rate and granular temperature for all three  $\langle f \rangle$ 's. In all cases, all of the particles show some tendency to concentrate to regions of low  $\overline{T}$ , low  $\dot{\gamma}$ , and high  $\overline{f}$  in the center of the chute, though the denser particles do so more effectively. In contrast with our results for different-sized particles [26], there is no segregation transition, or reversal, at intermediate solid fractions for different-density particles. This distinction may point toward an important difference in the segregation drivers of each at higher system solids fractions. We comment on this more in the conclusion section.

Additionally, we note that the degree of segregation in the steady state segregation patterns appears most pronounced for the intermediate value of  $\langle f \rangle$ ; in other words, qualitatively, the particles appear less segregated at the smallest and highest system solid fractions. This was also not observed in the case of mixtures of different sized particles, where, in the steady state segregation pattern, the segregation appeared equally-well pronounced for the mixtures of different sized particles for all solid fractions ( $\langle f \rangle = 0.2$  to  $0.6$ ) we investigated.

The profiles of the solids fraction and segregation fluxes for each component in Fig. 3

support the qualitative observations. We plot the solids fraction profiles  $\bar{f}_i$  of each component  $i$  ( $i = d$  for denser particles and  $i = l$  for less dense particles) and for the mixture  $\bar{f}$  at the steady state  $\langle f \rangle = 0.2, 0.4$ , and  $0.6$  in Fig. 3, row 1. The data for  $\bar{f}$  clearly shows the result of the migration of all particles to the center of the chute. At the larger values of  $\langle f \rangle$  (e.g.  $0.4$  or  $0.6$ ), the maximum local solids fraction of mixture is as high as  $0.71$ , close to hexagonal close packing. The relative segregation of the particles at steady state is also apparent in these plots. In all cases, the denser particles have a higher solids fraction in the middle region of the chute than the less dense particles; this is most pronounced for  $\langle f \rangle = 0.4$ , supporting our observations that segregation seemed most pronounced in the snapshots from  $\langle f \rangle = 0.4$  in Fig. 2.

Row 2 of Fig. 3 shows the profiles of the horizontal segregation fluxes  $\bar{f}_i \Delta \bar{v}_i = \bar{f}_i (\bar{v}_i - \bar{v})$  at the beginning of the simulations for these systems. For all three  $\langle f \rangle$ 's, the horizontal fluxes are strong and clear: the denser particles have positive fluxes in the left half of the chute and negative fluxes in the right half of the chute, indicating denser particles segregate to the center of the cell, while the less dense particles segregate to the walls. The relative

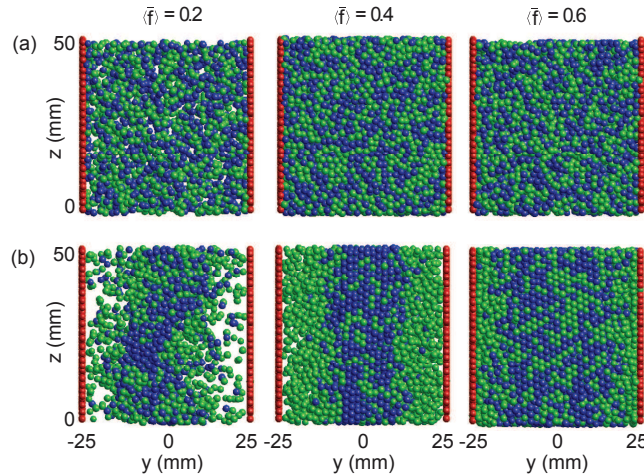


FIG. 2. (Color online) Snapshots of three mixtures at the beginning and steady state of each simulation. (The steady state time is determined using data plotted in Fig. 4.) (a) The beginning of the simulations ( $t = 0$  s). From left to right,  $\langle f \rangle = 0.2, 0.4$ , and  $0.6$ , respectively; (b) The steady state of the simulations. From left to right,  $\langle f \rangle = 0.2$  at  $t = 5$  s,  $\langle f \rangle = 0.4$  at  $t = 10$  s, and  $\langle f \rangle = 0.6$  at  $t = 300$  s, respectively. The different species are distinguishable by color: 2 mm denser particles, blue (dark); 2 mm less dense particles, green (light).

segregation fluxes decrease for higher values of  $\langle f \rangle$ , which is possibly due to a decrease of gradients of  $\dot{\gamma}$  and  $\bar{T}$  as  $\langle f \rangle$  increases [see Figs. 1(b)-(c)].

Row 3 of Fig. 3 shows the profiles of  $\bar{T}$  which we include because of its demonstrated importance in driving segregation in certain systems (e.g., [20, 21, 29]). In the sparse flow, the less dense particles have a higher value of  $\bar{T}$  than denser particles, which one might expect when considering momentum exchange among particles of different density (e.g., Ref. [37]). On the other hand, in the system of highest solids fraction ( $\langle f \rangle = 0.6$ ), the difference between species kinematic temperatures is minimal, especially at the center of the chute cell. This is consistent with our previous observations of highly concentrated mixtures in a drum [37], where we argued that in high solids fraction sheared flows, the velocity fluctuations did not differ for particles of similar size, regardless of their relative density because of geometric considerations of the particle movements.

We consider two quantities to determine the temporal evolutions of the mixture dynamics. The first is the width-averaged vertical velocity of the particles in the chute  $\langle w \rangle$ . We used

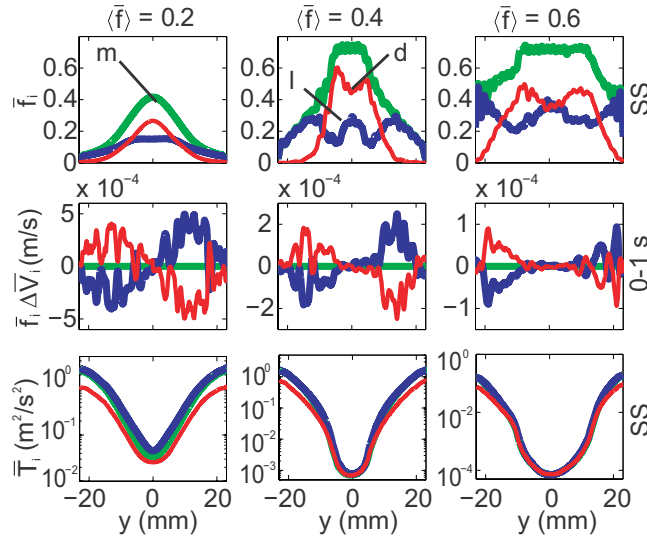


FIG. 3. (Color online) Segregation kinematics of three systems with  $\langle f \rangle$  as noted on top of each column for the mixture (m) [green (lighter line)] and dense (d) [red (darker line)] and less dense (l) [blue (Bold dark line)] particles. Row 1:  $\bar{f}_i$  at steady state (SS). Row 2: segregation fluxes  $\bar{f}_i \Delta \bar{V}_i$  as defined in text averaged over  $t = 0 - 1$  s (row 2). Row 3: kinematic granular temperature  $\bar{T}_i = (\overline{u_i' u_i'} + \overline{v_i' v_i'} + \overline{w_i' w_i'})/3$  at steady state. We note that the scales of the vertical axes in rows 2 and 3 vary for the different solid fractions.

230 this to estimate the time dependence of the average kinematics of the mixture. The second  
 231 measure we used provides a systematic measure of the rate and degree of segregation,  $S$ ,  
 232 essentially, the standard deviation of mean concentration  $S_i$  of each species  $i$  at each time  
 233 step  $t$ :

$$S_i(t) = \sqrt{\sum_{j=1}^{N_{bin}} [(\phi_i(t))_j - \langle \phi_i \rangle]^2 / (N_{bin} - 1)}. \quad (3)$$

234 Here,  $N_{bin} = 2500$  is the number of bins in the  $y$ -direction,  $(\phi_i(t))_j = (f_i/f)_j$  is the mixture  
 235 concentration of species  $i$  in bin  $j$  at time  $t$ , and  $\langle \phi_i \rangle = \langle f_i \rangle / \langle f \rangle$  is mean (volume) concen-  
 236 tration of this species in the system (0.5 for both species). Since  $\langle \phi_d \rangle = \langle \phi_l \rangle = 0.5$ , and  
 237  $(\phi_d(t))_j + (\phi_l(t))_j = 1$  (for all  $t$ ),  $S_d = S_l$ , which we denote by  $S$ .

238 Figure 4 shows the time-dependence of  $\langle w \rangle$  [Figs. 4 (a), (c), and (e)] and  $S$  [Figs. 4 (b),  
 239 (d), and (f)] for the same three systems presented in Figs. 2 and 3. For a sense of the spatial  
 240 resolution of the evolving segregation patterns in these systems, we plot the spatiotemporal  
 241 profiles of the concentration of the denser particles in Figs. 5 (a)-(d). In all systems at early  
 242 times,  $\langle w \rangle$  and  $S$  grow asymptotically from 0 to constant values, at which point the mean  
 243 flow kinematics and segregation reach a steady state. For  $\langle f \rangle = 0.6$ , this growth takes place  
 244 in two stages: first,  $\langle w \rangle$  and  $S$  increase to relatively constant values within a few seconds  
 245 and remain essentially steady until  $t \approx 100$  s [see Fig. 4 (e)]; then the particles suddenly  
 246 accelerate again and segregate further until another set of relatively constant values for  
 247  $\langle w \rangle$  and  $S$  is reached;  $\langle w \rangle$  and  $S$  remain steady once again until we stop the simulation at  
 248  $t \approx 300$  s [Fig. 4 (e)]. The time of this transition from one apparent metastable state to the  
 249 next differs with different initial conditions. We see evidence for a similar transition for our  
 250 moderate density system [ $t \approx 10$  s in Fig. 4 (c)], though the effect on segregation rate, if  
 251 any, is negligible [Fig. 4 (d)]. The re-acceleration of the flow is possibly due to a relatively  
 252 minor but sudden rearrangement of particles in the near-close-packed region similar to cage-  
 253 breaking in similarly dense sheared flows [38]. These dynamics could also be related to a  
 254 jamming transition, a matter that is currently under investigation.

255 To compare the rate for each system to reach steady state and the segregation rate at  
 256 different systems, we fit the curves of  $\langle w \rangle$  and  $S$  in Fig. 4 using one of two exponential  
 257 relations:

$$f(t) = A + B \exp(-t/\tau) \quad (4a)$$

$$g(t) = A + B \exp(-(t - t_0)/\tau) \quad (4b)$$

where fitting parameters  $A$  and  $B$  are the fitted initial ( $A + B$ ) and final ( $A$ ) values for each variable, and  $\tau$  is the timescale of each process. We fit the data from  $\langle f \rangle = 0.2$  and 0.4 using Equation (4a). During the first stage of  $\langle f \rangle = 0.6$ , we fit the variables using Equation (4a), and during the second stage (from  $t = 100$  to 300 s, determined empirically) we use Equation (4b), where  $t = 100$  s is our empirically-determined start time for the second stage of the system evolution.

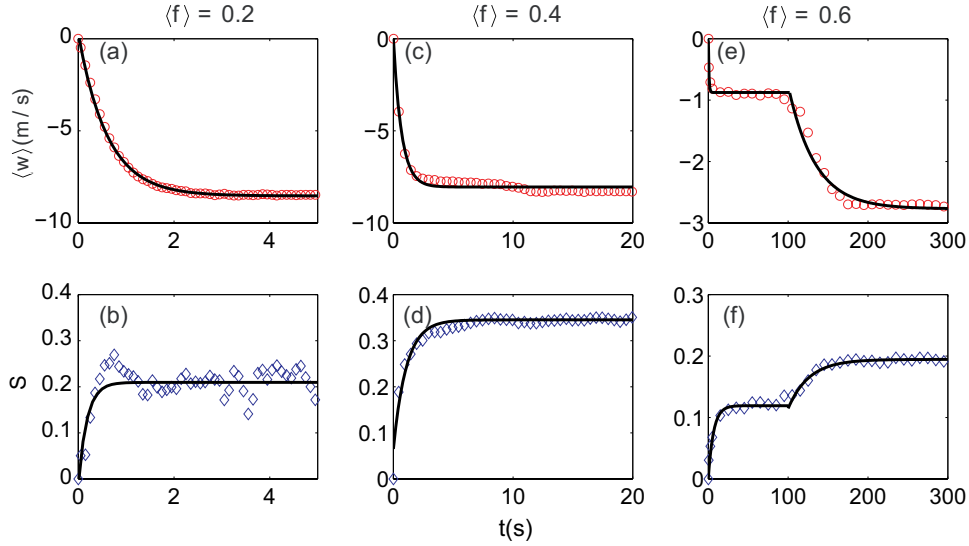


FIG. 4. (Color online) Time dependence of average downstream velocity  $\langle w \rangle$  and segregation index  $S$ : First row shows plots of the downstream velocity averaged across the width of the chute  $\langle w \rangle = \sum_{j=0}^{N_{bin}} \bar{f}_j \bar{w}_j / \sum_{j=0}^{N_{bin}} \bar{f}_j$ , where  $\bar{w}_j$  and  $\bar{f}_j$  are the average vertical velocity and average solid fraction of the mixture in bin  $j$  and  $N_{bin} = 2500$  is the number of bins in the  $y$ -direction and the second row shows plots of a measure of the segregation in the chute  $S$  [see Eq. (3)]. Symbols are data measured from DEM simulations and solid lines are exponential fits to the data. For  $\langle f \rangle = 0.2$  and  $0.4$ , the fit equations are  $f(t) = A + B \exp(-t/\tau)$ . For  $\langle f \rangle = 0.6$ , when  $t < 100$  s (stage I), the fit equation is the same as those at  $\langle f \rangle = 0.2$  and  $0.4$ , and when  $t > 100$  s (stage II), the fit equation is  $f(t) = A + B \exp(-(t - t_0)/\tau)$ . Here,  $A$ ,  $B$ ,  $t_0$ , and  $\tau$  are fitting parameters:  $A + B$  and  $A$  represent the initial and final values for each variable,  $\tau$  is the timescale, and  $t_0$  is indicative of the effective start time of the exponential decay during stage II for  $\langle f \rangle = 0.6$ . The fitting coefficients are shown in Table III.

TABLE III. Values of fitting coefficients for  $\langle w \rangle$  and  $S$ .

	$A_w$ (m/s)	$B_w$ (m/s)	$\tau_w$ (s)	$t_{0,w}$ (s)	$A_S$	$B_S$	$\tau_S$ (s)	$t_{0,S}$ (s)
$\langle f \rangle = 0.2$	-8.53	8.83	0.61	-	0.21	-0.22	0.18	-
$\langle f \rangle = 0.4$	-8.05	8.05	0.69	-	0.35	-0.28	1.08	-
$\langle f \rangle = 0.6(\text{I})^a$	-0.88	0.85	0.82	-	0.12	-0.12	6.60	-
$\langle f \rangle = 0.6(\text{II})^a$	-2.77	2.00	33.90	101	0.19	-0.077	26.22	100

<sup>a</sup> I and II represent two stages of the flow.

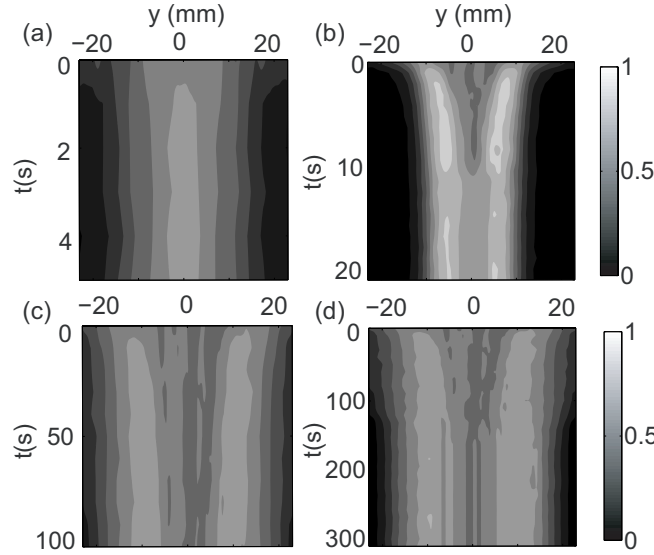


FIG. 5. Spatio-temporal profiles of concentration of denser particles ( $\phi_d = f_d/f$ ) for (a)  $\langle f \rangle = 0.2$  at  $t = 0 - 5$  s, (b)  $\langle f \rangle = 0.4$  at  $t = 0 - 20$  s, (c)  $\langle f \rangle = 0.6$  at  $t = 0 - 100$  s, and (d)  $\langle f \rangle = 0.6$  at  $t = 0 - 300$  s. The legend indicates the shade of gray that corresponds to particular fraction of denser particles. For example,  $\phi_d = 1$  for white pixels and  $\phi_d = 0$  for black pixels.

The values of these fitting parameters for  $\langle w \rangle$  and  $S$  for the three different  $\langle f \rangle$ 's are listed in Table III. The timescale for both  $\langle w \rangle$  and  $S$  ( $\tau_w$  and  $\tau_S$ , respectively) increase as  $\langle f \rangle$  increases, though the increase of  $\tau_w$  is not as pronounced as for  $\tau_S$ . The average flow in the sparsest system ( $\langle f \rangle = 0.2$ ), takes longer for the mean flow to reach the steady state than the essential segregation ( $\tau_w > \tau_S$ ). When  $\langle f \rangle$  increases to 0.4,  $\tau_w$  is comparable to  $\tau_S$ . For  $\langle f \rangle = 0.6$ ,  $\tau_S$  is 8 times larger than  $\tau_w$  in stage I, indicating segregation of the two species is still evolving when the mean flow has reached steady state.

As mentioned, segregation in the sparse system has been previously shown to be driven by the gradients of granular temperature, which can be modeled by the kinetic theory [21, 25]. We have shown that segregation can also be driven by gradients in shear rate and granular temperature gradients [26]. In Section IV A, we use a kinetic theory approach to model the shear-induced density segregation in the vertical chute. The kinetic theory captures the segregation trends and fluxes at sparse systems (e.g.  $\langle f \rangle = 0.2$ ), but it overestimates the segregation fluxes when the system concentration increases ( $\langle f \rangle \geq 0.4$ ). Next, we adapt a recently-developed theory [29] based on a mixture theory to understand the driving mechanisms for shear-induced density segregation for the higher  $\langle f \rangle$  systems.

## IV. TWO MODELS FOR SHEAR-INDUCED SEGREGATION

We consider these results in the context of two models. The first is kinetic theory for binary mixtures of slightly inelastic particles as detailed in Ref. [23]. The second is based on a model we previously proposed for different sized, same density particles, described in detail in Refs. [19, 29].

### A. Kinetic theory adapted for the vertical chute problem

To compare our simulation results with those predicted by kinetic theory, we consider that our particles are slightly dissipative (restitution coefficient  $e \approx 0.9$ ) and that what we might call the dynamic temperature of each species [the kinetic energy of the velocity fluctuations,  $T_D = m_i \overline{T}_i$  typically differ from one another ( $m_i$  is the mass of species  $i$ )]. As in Ref. [30], we use expressions derived under the framework of kinetic theory assuming a Maxwellian velocity distribution and allowing the particles to be slightly inelastic and that includes the effect of non-equipartition of temperature [37, 39, 40] according to expressions in Ref. [23] (similar to those in Ref. [20]).

To compare predictions from kinetic theory with our simulation results, we focus on segregation in the  $y$ -direction (see Fig. 2) within the first 1 s of the simulation. In Fig. 6, we plot the difference in the average “segregation” or “diffusion” velocities  $\overline{v}_l - \overline{v}_d$  of the two species from the DEM simulations and as predicted according to expressions developed from kinetic theory. (We note that the details on how the theoretical values are calculated



are included in Appendix A.)

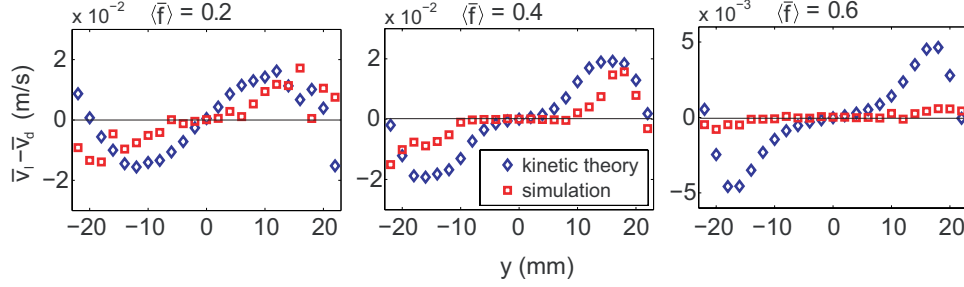


FIG. 6. (Color online) Profiles of the relative diffusion velocities  $\bar{v}_l - \bar{v}_d$  between less dense and denser particles in the  $y$ -direction averaged across the width of the chute and over the first 1 s for three different systems with  $\langle f \rangle$  indicated in the figure. Solid lines denote  $\bar{v}_l - \bar{v}_d = 0$  to guide eye.

In all cases, kinetic theory successfully predicts the segregation trend. Specifically, the dense particles segregate toward the center, and the less dense particles segregate toward the walls. For the sparse system ( $\langle f \rangle = 0.2$ ), kinetic theory successfully predicts the relative segregation velocities both qualitatively and quantitatively. The predicted fluxes are slightly larger than those measured from the simulation. This is probably due to the existence of “density waves” of locally high concentrations of particles as reported by Liss et al. [41] in this system (apparent in Fig. 2(b)), which is not accounted for in the development of the predictions we report here from kinetic theory (Appendix A). However, when the system is more concentrated ( $\langle f \rangle \geq 0.4$ ), kinetic theory over-predicts the relative segregation velocities. At  $\langle f \rangle = 0.6$ , the predicted segregation fluxes are one order of magnitude larger than fluxes from the simulation. These results indicate that kinetic theory can qualitatively predict segregation fluxes in agreement with previous work [21, 25]. However, as the system becomes more concentrated ( $\langle f \rangle > 0.4$ ), kinetic theory overestimates segregation fluxes as also found by Xu et al. [25], and the difference between theory and results increases as  $\langle f \rangle$  increases.

## B. Mixture theory with “temperature effects” adapted to density variations

We next consider a model we developed to account for the effect of temperature gradients on segregation in sheared high- $\langle f \rangle$  systems for particles differing only in size to determine whether or not it can be adapted to model the segregation effects we see here for mixtures



of particles differing in density. Our mixture theory model is more simplistic than kinetic theory in that it does not start at the particle-scale to develop rules for interactions between species. Rather, the interaction forces are based on some macroscopic assumptions of the mechanics of the interactions. In that way, this theory is more easily adaptable to different boundary conditions, but one must use caution in interpreting the results.

The basic form of the model is described in detail in Refs. [19, 29], adapted to gravity-driven flow in Ref. [42]. The model development in our earlier work was based, in part, on the assumption that the solids fraction  $f$  is uniform throughout for equal-density particles, and, therefore, so is what we might call the mixture *bulk density* defined by  $\rho = f\rho_m$ . For segregating mixtures of particles differing in material density, even if  $f$  is uniform,  $\rho$  becomes non-uniform as the mixture segregates. In this section, we outline our theory following much of the development we described in Refs. [19, 29], but modified to allow for a spatially varying particle density and then compare it with our DEM results.

### 1. Overview of mixture theory

As in the description for the DEM results, we denote bulk Eulerian properties of each species with subscripts and those of the mixture of both species together as variables without subscript (e.g.,  $\rho = \Sigma_i \rho_i$ , and  $\rho_i = \rho_{m,i} f_i$ ). We first consider conservation of mass and momentum for the mixture:

$$\frac{\partial \rho}{\partial t} + \nabla \cdot (\rho \mathbf{u}) = 0. \quad (5a)$$

$$\frac{\partial}{\partial t}(\rho \mathbf{u}) + \nabla \cdot (\rho \mathbf{u} \otimes \mathbf{u}) = \nabla \cdot \boldsymbol{\sigma} + \mathbf{F}. \quad (5b)$$

and the same for the individual species:

$$\frac{\partial \rho_i}{\partial t} + \nabla \cdot (\rho_i \mathbf{u}_i) = 0, \quad (6a)$$

$$\frac{\partial (\rho_i \mathbf{u}_i)}{\partial t} + \nabla \cdot (\rho_i \mathbf{u}_i \otimes \mathbf{u}_i) = \nabla \cdot (\boldsymbol{\sigma}_i) + \mathbf{F}_i + \boldsymbol{\beta}_i. \quad (6b)$$

In these equations,  $\boldsymbol{\sigma}$  is the stress tensor using the relatively standard sign convention for stresses as, for example, noted in Ref. [43], and  $\mathbf{F}$  represents the net body force per unit

341 volume.  $\sigma_i$  is the local stress borne by species  $i$ , and the total stress  $\sigma = \sum \sigma_i$ .  $\beta_i$  represents  
 342 the interaction force exerted on species  $i$  by the other species.

343 We then consider the instantaneous value of each variable  $q$  at position  $\mathbf{r}$  as a sum of  
 344 the local temporal average  $\bar{q}(\mathbf{r})$  and the difference between its instantaneous value and the  
 345 average  $q'(\mathbf{r}, t) = q(\mathbf{r}, t) - \bar{q}(\mathbf{r})$  (typically called ‘‘Reynolds decomposition,’’ [44]). We consider  
 346 the results in the context of pseudo-2d systems like the vertical chute so that the flow exhibits  
 347 uniformity in the directions perpendicular to segregation (e.g.  $x$ – and  $z$ –directions). We  
 348 rewrite the momentum equation (5b) for the mixture in the  $y$ – direction as

$$\frac{\partial}{\partial t}(\bar{\rho} + \rho')(\bar{v} + v') + \frac{\partial}{\partial y}[(\bar{\rho} + \rho')(\bar{v} + v')(\bar{v} + v')] = \frac{\partial}{\partial y}(\bar{\sigma}_{yy} + \sigma'_{yy}) + \bar{F}_y + F'_y \quad (7)$$

349 We consider systems in which the mixture velocity reaches steady state (as in the majority  
 350 of the segregation for  $\langle f \rangle = 0.6$  in Fig. 4, row 3). We approximate the correlations between  
 351 velocity fluctuations and concentrations as negligible (as we found in Ref. [29]). Finally, for  
 352 this paper, we restrict our discussions to cases where the only body force (particle weight)  
 353 is in the  $z$ –direction, like the vertical chute. Then the Reynolds averaged equations in the  
 354  $y$ –direction may be expressed as :

$$\frac{\partial \bar{\sigma}_{yy}^c}{\partial y} + \frac{\partial \bar{\sigma}_{yy}^k}{\partial y} = 0, \quad (8)$$

355 for the mixture and

$$\frac{\partial \bar{\sigma}_{yy,i}^c}{\partial y} + \frac{\partial \bar{\sigma}_{yy,i}^k}{\partial y} - \bar{\beta}_{y,i} = 0. \quad (9)$$

356 for the individual components. As in Ref. [29], we refer to  $\bar{\sigma}_{yy}^k \equiv \overline{\rho v'v'}$  as a component of  
 357 the kinetic stress and define a contact stress tensor  $\sigma^c = -\sigma$  so that terms such as  $\bar{\sigma}_{yy}^c$  are  
 358 positive for our problem where there are only compressive, not tensile, interactions between  
 359 particles. We note that  $\overline{\rho v'v'}$  scales roughly with  $T$ , so that Eq. (8) indicates that a gradient  
 360 in  $T$  can be associated with a gradient in both  $\bar{\sigma}_{yy}^k$  and  $\bar{\sigma}_{yy}^c$  (of opposite signs). Since all  
 361 terms in Eqs. (8) and (9) are averaged, we drop the overbar from this point in this paper,  
 362 so that unless noted for each variable  $q$  alone refers to the average quantity  $\bar{q}$ .

363 In contrast with classic mixture theory (e.g., Refs. [45–47]), we follow Refs. [29, 42]  
 364 and references within, and allow the partitioning of kinetic and contact stresses between the  
 365 species to vary from the associated solids fractions ( $\sigma_{yy,i}^c \neq \phi_i \sigma_{yy}^c$  and  $\sigma_{yy,i}^k \neq \phi_i \sigma_{yy}^k$ ). Instead,  
 366 we use independent stress partition coefficients ( $\psi_i^c$  and  $\psi_i^k$ ):

$$\sigma_{yy,i}^c = \psi_i^c \sigma_{yy}^c, \text{ and } \sigma_{yy,i}^k = \psi_i^k \sigma_{yy}^k, \quad (10)$$

where  $\psi_i^{\mathbf{c}}$  and  $\psi_i^{\mathbf{k}}$  determine the proportion of normal contact and kinetic stresses carried by species  $i$  and are not necessarily equal to  $\phi_i$ .

For the interaction term  $\beta_{y,i}$ , we propose a similar form to that for equal density particles in Ref. [29], modified slightly to account for the variable species concentrations throughout the system:

$$\beta_{y,i} = \sigma_{yy}^{\mathbf{c}} \frac{\partial}{\partial y} \psi_i^{\mathbf{c}} + \sigma_{yy}^{\mathbf{k}} \frac{\partial}{\partial y} \psi_i^{\mathbf{k}} - \rho_i c_D (v_i - v) - d \frac{\partial \rho_i}{\partial y}, \quad (11)$$

The first two terms on the right hand side of the equation ensure that, as in Darcy’s law, the segregation process is driven by intrinsic rather than partial stress gradients (as in Refs. [47–49]). The third term is a linear drag law, and  $c_D$  is a linear drag coefficient. The fourth term acts as a “remixing force” that drives grains of constituent  $i$  towards areas of lower concentration, and  $d$  is an ordinary diffusion coefficient.

Combining Eqs. (10)-(11) with Eq. (8), a segregation flux of species  $i$  can be expressed as:

$$\rho_i (v_i - v) = \frac{(R_i^{\mathbf{c}} - R_i^{\mathbf{k}}) \phi_i}{c_D} \frac{\partial \sigma_{yy}^{\mathbf{k}}}{\partial y} - \frac{d}{c_D} \frac{\partial \rho_i}{\partial y}. \quad (12)$$

$R_i^{\mathbf{c}} = \psi_i^{\mathbf{c}}/\phi_i$  and  $R_i^{\mathbf{k}} = \psi_i^{\mathbf{k}}/\phi_i$  are stress partition variables we introduce to facilitate a physical interpretation of the governing features of this equation. Equation (12) is similar to, but more general than, the equivalent expression for equal density particles presented as Equation (11) in Ref. [29] as:

$$\phi_i (v_i - v) = \frac{(R_i^{\mathbf{c}} - R_i^{\mathbf{k}}) \phi_i}{\rho c_D} \frac{\partial \sigma_{yy}^{\mathbf{k}}}{\partial y} - \frac{d}{c_D} \frac{\partial \phi_i}{\partial y}. \quad (13)$$

For mixtures of particles of the same material density,  $\rho$  can be expressed by  $\rho = \rho_m f$ , where  $\rho_m$  is the material density of *all* species in the mixture, so the two expressions for flux are interchangeable. For our mixtures of particles of different densities  $\rho = \rho_{m,d} f_d + \rho_{m,l} f_l$ , and the two expressions for flux are not equal.

Otherwise, the predictions are similar. Both Equations (12) and (13) predict that if  $R_i^{\mathbf{c}} = R_i^{\mathbf{k}}$ , the species will not segregate. However, if  $R_i^{\mathbf{c}} \neq R_i^{\mathbf{k}}$  and  $\partial \sigma_{yy}^{\mathbf{k}}/\partial y \neq 0$ , whichever species carries a higher fraction of the contact stress than they do the kinetic stress should be pushed to the region of higher temperature.

To compare the theoretical predictions with the computational results, we consider that, for the theoretical development, we have assumed that the velocities in the system reach steady state before the majority of the segregation process takes place. This condition is met for the initial segregation that occurs for the highest,  $\langle f \rangle \sim 0.6$ , so we focus our comparison on this case. We do not have a predictive form for stresses or the coefficients of drag and diffusion. In lieu of a direct comparison of theory and simulation, we investigate the relationships between the segregation flux and partition coefficients measured in the simulations and compare them with those predicted by Equation (12) to determine whether the theoretical framework is consistent with the simulations. Then we use these data to obtain estimates for the coefficients of drag and diffusion as described shortly.

We first calculate the stresses and other dynamics in the simulations throughout the system including the partition coefficients for the partial stresses and the concentration profiles. For the stresses, we follow the same procedure described in Ref. [29], which we summarize in Appendix B. We have found that the stresses do not change considerably over the course of the simulation and plot the profiles from the data averaged over  $t = 50$ - $100$  s in the simulation after the mixture kinematics first reach a quasi-steady state. In Fig. 7 (a), we plot the profiles of  $\sigma_{yy}^k(y)$  and  $\sigma_{yy}^c(y)$ , which in many ways are similar to those using equal-density, different-sized particle mixtures in Ref. [29]. The profile of  $\sigma_{yy}^k(y)$  peaks near the rough walls and dips in the middle. As one would expect from Eq. (8),  $\sigma_{yy}^c(y)$  follows the opposite trend: it is highest in the middle and dips near the walls. The total stress  $\sigma_{yy}^c(y) + \sigma_{yy}^k(y)$  is nearly constant across the chute cell. We fit the data by exponential functions:  $\sigma_{yy}^k(y) = A \exp(B|y|)$ , and  $\sigma_{yy}^c(y) = C - A \exp(B|y|)$ , where the fitting parameters are given in the caption of Fig. 7. Figures 7 (b) and (c) show the contact and kinetic stresses associated with each of the two species, and Fig. 7 (d) shows the concentration profiles of each constituent in the  $y$ -direction. These results indicate that, depending on the region of the chute, either the less dense or the denser particles may take up a higher fraction of the local stress, and  $\sigma_{yy,i}^c(y)$  scales most closely with  $\phi_i(y)$ .

In Fig. 8 we plot the relative partial stress coefficients  $R_i^c = \psi_i^c/\phi_i$  and  $R_i^k = \psi_i^k/\phi_i$ , averaged over the time interval  $t = 50 - 100$  s.  $R_i^c \approx 1$  except immediately adjacent to the wall, where the results may be affected by the neighboring wall particles. These results

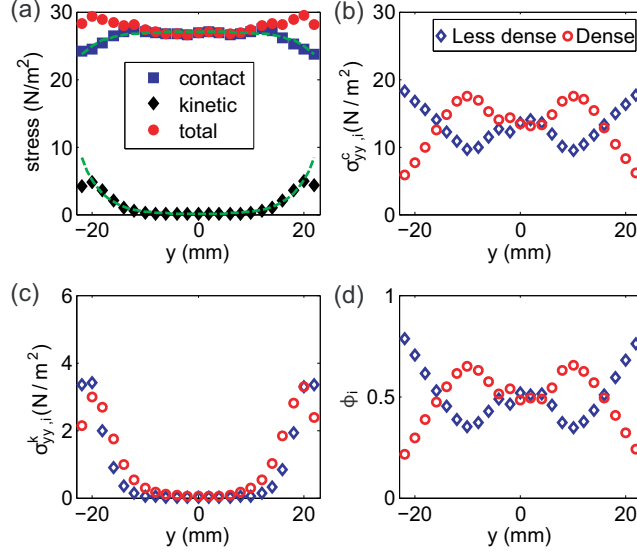


FIG. 7. (Color online) The  $y$ -component of total and partial normal stresses in the  $y$ -direction for the mixture and the two species at a quasi-steady state ( $t = 50 - 100$  s). (a) total, kinetic, and contact stresses for the mixture; (b) contact stresses for the two species; (c) kinetic stresses for the two species; (d) species concentrations. The dashed lines in (a) are exponential fits for the kinetic and contact stresses of the mixtures. For kinetic stresses:  $\sigma_{yy}^k(y) = A \exp(|By|)$  based on a linearized least squares fit, where  $A = 3.6 \times 10^{-2}$  N/m<sup>2</sup> and  $B = 0.25$  mm<sup>-1</sup>; for contact stresses:  $\sigma_{yy}^c(y) = C - A \exp(|By|)$ , where  $A = 1.6 \times 10^{-2}$  N/m<sup>2</sup>,  $B = 0.24$  mm<sup>-1</sup> and  $C = 27.05$  N/m<sup>2</sup>.

indicate that nearly everywhere the contact stress borne by each species is proportional to its local concentration, i.e.,  $\psi_i^c = \phi_i$ . In contrast, the denser particles carry a significantly higher fraction of the kinetic stresses than their concentration ( $R_d^k > 1$ , and  $\psi_d^k > \phi_d$ ), and the less dense particles carry a lower fraction of the kinetic stresses than their concentration ( $R_l^k < 1$ , and  $\psi_l^k < \phi_l$ ). We briefly note here that these results are markedly different than in mixtures of particles differing only in size, where the lighter (smaller) particles carry a higher fraction of the kinetic stress [29, 42]. We discuss this more in Sections V and VI.

The results in the mixtures of particles differing only in density indicate that  $R_l^c - R_l^k > 0$  and  $R_d^c - R_d^k < 0$ . Considering this in the context of the theoretical predictions in Equation 12, the less dense particles should migrate in the direction of increasing kinetic stress and the denser particles should migrate in the direction of decreasing kinetic stress (Fig. 8(c)). Since  $\partial \sigma_{yy}^k / \partial y > 0$  for  $y < 0$  and  $\partial \sigma_{yy}^k / \partial y < 0$  for  $y > 0$  [see Fig. 7(a)], Eq. (12) predicts

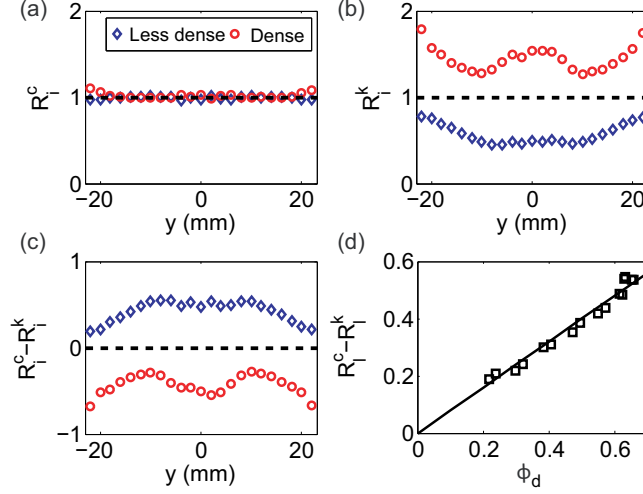


FIG. 8. (Color online) Profiles of partial stress coefficients  $R_i^c$  (a) and  $R_i^k$  (b) averaged at  $t = 50 - 100$  s. (c) Profiles of  $R_i^c - R_i^k$ . (d) A parametric plot from the data shown in (c) and Fig. 7(d) for  $R_L^c - R_L^k$  vs.  $\phi_D$ . The dashed lines in (a)-(c) are used to indicate the case where  $R_i^{k,c}=1$  for both components, i.e., indicating the values on the plot for which the stresses would be equally partitioned between the components. The solid line in (d) is a linear least-squared fit for  $R_L^c - R_L^k = B\phi_D$ ;  $B \approx 0.8$ .

that denser particles segregate to the center of the cell and the less dense particles segregate to the walls, consistent with our simulation results (e.g., Figs. 2(c) and 3).

We build on these results to develop a prediction for the evolution of the local concentrations of the species. We first consider the equation of conservation of mass for species  $i$ . With no gradients in the  $x$ - and  $z$ -directions and assuming the solids fraction of the mixture is time independent during segregation ( $\partial f / \partial t = 0$ ), we can rewrite Eq. (6a) as:

$$\rho_{m,i} f \frac{\partial \phi_i}{\partial t} + \frac{\partial}{\partial y} (\rho_i v_i) = 0. \quad (14)$$

We substitute the theoretical form of the segregation flux expressed in Eq. 12 into Eq. 14, and we find:

$$\rho_{m,i} f \frac{\partial \phi_i}{\partial t} + \frac{\partial}{\partial y} \left( \frac{(R_i^c - R_i^k) \phi_i}{c_D} \frac{\partial \sigma_{yy}^k}{\partial y} - \frac{d}{c_D} \frac{\partial \rho_i}{\partial y} \right) = 0. \quad (15)$$

Comparing the concentration profiles in Fig. 7(d) with profiles of  $R_i^c - R_i^k$  in Fig. 8(c) indicates that the magnitude of  $R_i^c - R_i^k$  for each species is correlated with the concentration of the other species. We plot  $R_i^c - R_i^k$  vs.  $\phi_d$  for these data in Fig. 8(d) excluding the creeping regions in the middle of the chute ( $-6\text{mm} < y < 6\text{ mm}$ ). Though not perfectly linear [see

fit in Fig. 8(d)], we approximate it as such in Equation 15, i.e.,  $R_l^c - R_l^k \approx B\phi_d$ , where  $B$  is a fitting parameter. (We determined that  $B \approx 0.8$  by fitting the data in Fig. 8). Then Eq. (15) may be rewritten for the less dense particles as:

$$\frac{\partial \phi_l}{\partial t} + \frac{B}{c_D \rho_{m,l} f} \frac{\partial}{\partial y} \left[ \phi_l (1 - \phi_l) \frac{\partial \sigma_{yy}^k}{\partial y} \right] - \frac{d}{c_D f} \frac{\partial^2 f \phi_l}{\partial y^2} = 0. \quad (16)$$

The spatio-temporal profiles of concentration of less dense particles can then be obtained by solving Eq. (16) numerically, though  $f(y)$ ,  $\partial \sigma_{yy}^k / \partial y$ , diffusivity  $D = d/c_D$ , and the ratio  $q = B/c_D$  (an indication of the segregation magnitude) must be obtained. For  $f(y)$  and  $\partial \sigma_{yy}^k / \partial y$  we use the profiles of the mixture solid fraction [Fig. 1(d)] and normal kinetic stresses in the  $y$ -direction [Fig. 7(a)] obtained from the simulations. We do not know  $D$  and  $q$ ; for simplicity, we choose constant values for these two parameters empirically by comparing the predictions obtained using different values of  $D$  and  $q$  to the simulation results. For our numerical solution, we use initial conditions consistent with a homogenous mixture ( $\phi_d = \phi_l = 0.5$  at  $t=0$  for all values of  $y$ ), and no-flux conditions at the two walls ( $-q(1 - \phi_l)\phi_l(\partial \sigma_{yy}^k / \partial y) / \rho_{m,l} = D \partial(f\phi_l) / \partial y$  at  $y = \pm 25$  mm for all values of  $t$ ). We then discretize the problem and solve numerically by using a central difference scheme for spatial derivatives and modified Euler method for time integration.

Figure 9 shows spatio-temporal profiles of concentration of less dense particles from theoretical predictions up to 300 s. Based on trial and error we chose  $q = 1 \times 10^{-3}$  s and  $D = 0.2$  mm<sup>2</sup>/s. The value for  $D$  is similar to that we found for a mixture of 2 mm and 3 mm particles in a drum, where we found  $d = 1.26 \times 10^{-5}$  m<sup>2</sup>/s<sup>2</sup> and  $c_D = 6.3$  s<sup>-1</sup> so that  $D \approx 0.2$  mm<sup>2</sup>/s. On the other hand  $c_D = B/q = 0.8/(10^{-3} \text{ s}) = 80$  s<sup>-1</sup> is significantly larger than that for the mixture of different sized particles ( $\approx 6.3$  s<sup>-1</sup>). It is likely that both  $D$  and  $c_D$  vary with details such as the local shear rate as in Ref. [13, 28, 50], so that such comparisons are not so useful, but rather the next generation of the model should consider a more physically representative form for these parameters which we discuss in the next section.

In both the theoretical predictions and simulation results [compare Fig. 9 (a) and (b) with Fig. 5 (c) and (d), respectively], the less dense particles segregate to the side walls, and dense particles segregate toward the center. In the middle of the chute, in the slow creeping region where the gradients of normal kinetic stresses is very small, the segregation

475 process is much slower than other regions. All of these indicate a good qualitative agreement  
 476 between theoretical predictions and simulation results. On the other hand, the theory does  
 477 not capture the sudden intensifying of the segregation pattern that begins  $\approx 100$  s in the  
 478 simulations that appears to be correlated with an increase in average velocity. We hypoth-  
 479 esize this sudden change is associated with an increase in packing efficiency and decrease in  
 480 relative magnitude of collisional damping of the particle motion that is not captured by the  
 481 theory.

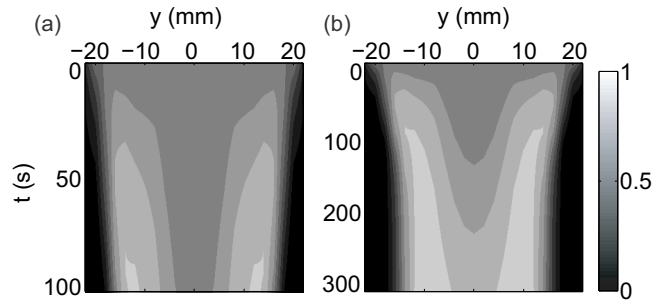


FIG. 9. Theoretical predictions of spatio-temporal profiles of the concentration of less dense par-  
 ticles compared to those in Figs. 5 (c) and (d). (a)  $t = 0 - 100$  s (b)  $t = 0 - 300$  s. The legend  
 indicates the shade of gray that corresponds to particular fraction of denser particles. For example,  
 $\phi_d = 1$  for white pixels and  $\phi_d = 0$  for black pixels.

482 Finally, with the fitted values of  $q$  and  $D$  from above, we compare the segregation velocity  
 483  $v_l - v_d$  predicted by Eq. (12) with the simulation results for the first second and at the steady  
 484 state ( $t = 300 - 310$  s), as shown in Fig. 10. Our theoretical predictions match well with  
 485 DEM simulations at both stages of simulations, in contrast to the kinetic theory (Fig. 12),  
 486 which, based on the local kinematics in the DEM simulations, overpredicts the segregation  
 487 velocity by approximately one order of magnitude compared with that exhibited by the  
 488 DEM simulations.

## 489 V. DISCUSSION

490 These results add to the growing body of evidence supporting the importance of veloc-  
 491 ity fluctuations (via granular temperature and/or kinetic stresses) in driving segregation in  
 492 high solids fraction granular flows. Effects of velocity fluctuations are typically discounted



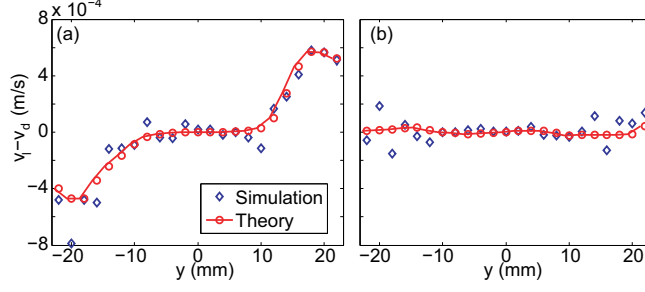


FIG. 10. (Color online) Comparison of profiles of segregation velocity  $v_l - v_d$  vs.  $y$  between theoretical predictions from Eq. (12) and DEM simulations at (a) the first second and (b)  $t = 300 - 310$  s for  $\langle f \rangle = 0.6$ .

in high- $f$  granular flows as they are relatively small. For example, kinetic stress is much smaller than contact stress (e.g., Fig.7), and the kinetic energy associated with velocity fluctuations is much smaller than gravitational potential energy differences in a granular mixture. The results reported here support the premise that, even though velocity fluctuations are relatively small compared with other dynamics in high- $f$  flows, *gradients* of kinetic stress can drive segregation in a wide variety of granular materials at high solids fractions (high- $f$ ). Specifically, the kinetic stresses drive the segregation direction and magnitude through: (1) the manner in which they are partitioned among different species compared to the partitioning of contact stresses and (2) the gradient in the kinetic stresses. These results are qualitatively similar in mixtures of particles differing only in size and those differing only in density.

A striking difference between the segregation of mixtures of different sized particles and different density particles in high- $f$  flow is the segregation direction of the more massive particles. The direction of segregation of the more massive (denser) particles in mixtures of particles differing only in density is opposite to the more massive (larger) particles in mixtures of particles differing only in size. In the first case, the more massive (denser) particles segregate along a kinetic stress gradient toward the region of lower kinetic stress, and in the second case, the more massive (larger) particles segregate toward the region of higher kinetic stress. Our results indicate that this difference is driven by the manner in which the kinetic stress is partitioned among the different species. In high- $f$  flows, the smaller particles bear a higher fraction of the kinetic stress than their larger equal-density counterparts [19, 29, 30, 37], and the denser particles bear a higher fraction of the

kinetic stress than their lighter equal-sized counterparts (similar to results in Ref. [37]). Previously published results (e.g., Ref. [37]) suggest these differences are driven primarily by the geometry of correlated particle movements in these high- $f$  flows, so, interestingly, it appears the geometry driving the fluctuations in these high- $f$  flows is a significant contributor to the segregation in these systems.

Once the kinetic stress is unevenly distributed among the species, the species that bear a larger fraction of the kinetic stress than their volume concentration in the mixture are driven toward “cooler” regions (those of lower kinetic stress and lower granular temperatures). Those that bear a smaller fraction of the kinetic stress are driven toward “hotter” regions (those of higher kinetic stress and higher granular temperatures). It is not immediately obvious why this occurs, but for insight we might consider that all particles appear driven away from high-temperature regions. If one species bears a higher fraction of the kinetic stress than the other, the additional random kinetic energy may allow that species to explore more pore spaces among the mixture to get to the lower temperature regions.

We have shown here and elsewhere ([19, 30]) that kinetic theory, perhaps the most complete physics-based predictive theoretical frameworks for granular mixtures breaks down in its prediction of segregation in high- $f$  flows. While kinetic theory directly accounts for particle scale interactions in the form of transfer of momentum, and energy during collisions, the predictions are based on the assumption that collisions are chaotic, uncorrelated, and binary. Effects due to simultaneous multi-particle interactions are typically not captured, though there have been some recent attempts to extend kinetic theory by considering macroscopic structures in granular flows [51]. The need to account for these effects may be responsible for the breakdown in kinetic energy predictions at higher solids fraction. We are currently investigating these questions in detail, as they may also prove relevant for the results we present here where small scale rearrangements can apparently lead to large scale system segregation adjustments.

Other than kinetic theory, relatively little theoretical investigation has been performed for the manner in which gradients in velocity fluctuations, granular temperature, and kinetic stresses may drive segregation. The theory described here shows promise in its ability to capture segregation in these systems. In the end, it is a relatively simple but critical generalization of the theory presented in Refs. [19, 29]. We note that the theory suffers from empirical expressions for drag and diffusion coefficients, and other details of the interparticle

interactions. In that light, it is interesting to consider the empirical results with those from other models. Most relevant for the mixtures discussed here, Tripathi and Khakhar [27, 28] proposed a form for the drag force analagous to Stoke’s Law. Additionally, the extended form of kinetic theory proposed by Larcher and Jenkins [51] has alternative forms for the drag and diffusion coefficients that could be tested for their effectiveness in application to this mixture theory.

## VI. CONCLUSION

In this paper, we performed a numerical and theoretical study of segregation of particles differing only in density sheared in a vertical chute cell. We showed that gradients in the shear rate and associated kinematics in the span-wise direction can drive segregation by particle density in both sparse and high solids fraction systems. This shear-induced segregation, reported for high solids fractions mixtures of particles differing only in density for the first time, exhibits a similar segregation trend to previous reports of analogous phenomena in sparse flow. Specifically, the denser particles segregate to the region of a lower shear rate and granular temperature, and the less dense particles segregate to the region of higher shear rate and granular temperature. This is in stark contrast to our previous observations of shear-induced segregation of particles differing only in size [26] which exhibits a phase transition at intermediate concentrations. In sparse flows large particles segregate to regions of low shear rates, low granular temperatures, and low kinetic stress, while in high solids fraction flows, large particles segregate to regions of high shear rates, high granular temperatures and high kinetic stresses. This dichotomy may be related to recent reports of an intermediate segregation state in mixtures of particles differing both in size and density where particles that are both larger and denser than their smaller less dense counterparts rise to an intermediate level in a sheared system where the shear rate is non-uniform (e.g., Refs. [12, 52–54]).

Our mixture theory successfully predicts the segregation trends observed in the simulations, though, admittedly, uses empirical fits for some of the coefficients. In the framework of this theory, the shear rate gradients give rise to kinetic stress gradients – closely related to the gradients of granular temperature – which explicitly drive density segregation. Then, the particles which bear more of the contact stress than the kinetic stress – here, the less

dense particles – are pushed to the regions of low contact stress and high kinetic stress (or high granular temperatures). In contrast, in high solids fraction mixtures of particles differing only in size, the large particles bear more of the contact stress than the kinetic stress and push the large particles to the regions of low contact stress and high kinetic stress (or high granular temperature).

Although the framework is reasonable for shear-induced segregation, and predictions appear to correlate reasonably well with observations, a deeper understanding of the kinematics of high- $f$  sheared mixtures is needed for a complete segregation theory. First, we need a relationship between  $R_i^c - R_i^k$  and flow properties such as particle concentrations and flow velocities to close the governing equations. For this, we have temporarily used a linear relationship between  $R_i^c - R_i^k$  and  $\phi_j$  (for disparate species  $i$  and  $j$ ), though this is clearly not completely representative, judging from the data (Fig. 8(d)). Coefficients of drag and diffusion also suffer from this empirical over-simplified nature. A more mechanistic way to obtain relationships for  $D$  and  $c_D$  as they depend on kinematics of the flow is necessary for a predictive model for shear-induced segregation.

Finally, most segregation takes place in a gravitational field where segregation may be driven by simultaneous effects associated with the gravity and shear rate gradients. A more widely-applicable theory will combine the theoretical details described in this paper and in Ref. [29] with gravity-driven segregation effects, such as those described by Gray and colleagues, first in Refs. [48, 49] or Khakhar and colleagues, first in Ref. [10], and more recently in Refs. [13, 27, 28]. Preliminary results presented in Ref. [42] show promise in capturing the simultaneous effects of particle size and density in segregating mixtures.

## ACKNOWLEDGMENTS

We are grateful for the financial support of: NSF CMS-0625022 and NSF CBET-0932735.

## Appendix A: Kinetic theory expressions used in segregation prediction

As in Refs. [20, 23, 30], The diffusion velocity of two species  $i$  and  $j$  in the direction of the interest (e.g.  $y$ -direction) can be calculated as:

$$v_i - v_j = -\frac{n^2}{n_i n_j} D_{ij} d_i, \quad (\text{A1})$$

Where,  $D_{ij}$  is the local coefficient of diffusion, and  $d_i$  (sometimes called a “diffusion force” [22]) represents competing segregation and mixing factors leading to the difference in diffusion velocities ( $v_i - v_j$ ) and subsequent segregation between the two types of particles. Calculations performed for  $D_{ij}$  and  $d_i$  are listed in Table IV. The calculations involve terms related to granular temperature  $T_D$ , pressure  $P$  and ordinary diffusion represented by  $d_T$ ,  $d_p$ , and  $d_n$ . We note that the granular temperature used here is what might be considered a *dynamic* granular temperature compared with the temperature plotted in Fig. 3:  $T_{D,i} = m_i T_i$ . Also, pressure  $P_i$  is distinct from the hydrostatic pressure and is derived from considerations within the framework of kinetic theory and conservation of momentum for the two species as shown in Refs. [20, 23].

We average the details in the  $x$ - and  $z$ -directions over the first 1 s of the experiment. In our calculations, most of the variables, such as  $T_D$ , are calculated directly from the simulations directly, while the initial solids fraction of each species is set to be uniform, each equal to one half of the total solids fraction ( $f_i(y) = \langle f \rangle / 2$ ).

The first column of Fig. 11 shows the profiles of  $T_D(y)$  for the two constituents at three different  $\langle f \rangle$ 's. In all systems,  $T_D$  is large close to the walls and small at the center of the cell for both species (similar to Fig. 3, row 4). As  $\langle f \rangle$  increases from 0.2 to 0.6, temperature gradients decrease approximately by two orders of magnitude. Furthermore, the less dense component always has greater values of  $T_D$  than denser particles in the regions close to the walls, where the flow is dilute [see Fig. 1(d)]. In contrast,  $T_D$  are roughly the same in the region at the center of the cell, where the flow is highly concentrated. This matches the observation for the flow of granular mixtures differing only in density in the rotating drums [37]: granular temperature scales inversely only with size, not with density in high- $f$  regions, while in low- $f$  regions, granular temperature scales inversely with mass (or material density for same size particles). The second column of Fig. 11 shows profiles of  $P(y)$ . Similar to  $T_D$ ,  $P$  is large in the region close to the walls and small in the region at the center of the

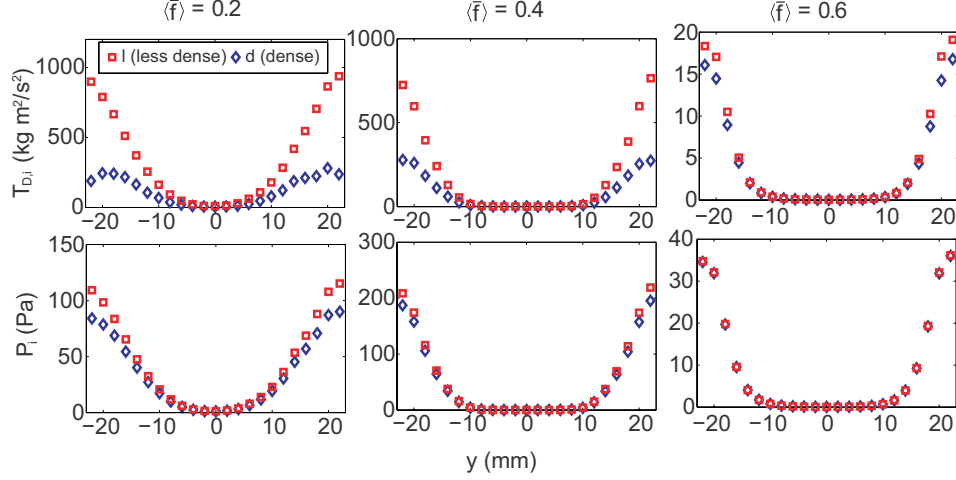


FIG. 11. (Color online) Profiles of Dynamic granular temperature and dynamic pressure for two species in the  $y$ -direction averaged across the width of the chute and over the first 1 s for three systems of different  $\langle f \rangle$ 's as indicated in the figure. First row: Plots of dynamic granular temperature  $T_D$ ; Second row: Plots of dynamic pressure  $P$ .

cell. The pressure of less dense particles is larger than dense particles in the dilute region. In the high- $f$  region, the pressure of two species are almost the same.

The second column of Fig. 12 shows the diffusion forces that drive the segregation and diffusion fluxes (as calculated in Table IV). Based on Eq. (A1), positive (negative) diffusion forces in the left (right) half of the chute cell imply negative (positive) values of  $v_l - v_d$ , indicating less dense particles segregate to the side walls. In all three systems, the thermal ‘diffusion force’,  $d_T$ , that is associated with gradients of the granular temperature is much greater than the other two diffusion forces (i.e.  $d_n$  and  $d_p$ ), indicating that  $d_T$  is the dominating driving forces for density segregation in vertical chute flow. However, as shown in Fig. 6, the kinetic theory overpredicts  $v_l - v_d$  at high  $f$  compared with the DEM simulation, which implies that the thermal driven ‘diffusion force’ as calculated in Table IV probably overestimates the granular temperature gradient effects on density segregation in high- $f$  granular flow.

## Appendix B: Stress calculation

In this Appendix, we briefly describe our calculations of the total and partial stresses we use for testing our theoretical segregation predictions for the mixture theory. To do so, we

TABLE IV. Variables in the diffusion equation [Eq. (A1)] of kinetic theory

Variable	Expression	Description
$r_i$	$r_i$	Particle radius of species $i$
$m_i$	$m_i$	Particle mass of species $i$
$n_i$	$\frac{f_i}{4\pi r_i^3/3}$	Number density of species $i$
$T_{D,i}$	$m_i T_i = m_i \frac{u'_i u'_i + v'_i v'_i + w'_i w'_i}{3}$	<i>Dynamic</i> granular temperature of species $i$
$P_i$	$n_i(T_{D,i} + \Delta T_{D,i}) + \sum_{k=1}^2 K_{ik} \left[ T_{D,i} + \frac{(m_i \Delta T_{D,k} + m_k \Delta T_{D,i})}{(m_i + m_k)} \right]$	<i>Dynamic</i> granular pressure of species $i$
$d_i$	$d_P + d_T + d_n$	“Diffusion force” for species $i$
$d_P$	$\frac{\frac{P_j}{P_i} \nabla P_j - \nabla P_i}{n T_D \left( \frac{P_j}{P_i} + 1 \right)}$	Pressure driven diffusion force
$d_T$	$-\frac{K_{ij}}{n T_D} \frac{m_j - m_i}{m_j + m_i}$	Thermal driven diffusion force
$d_n$	$-\frac{K_{ij}}{n} \left[ \frac{\nabla n_i}{n_i} - \frac{\nabla n_j}{n_j} \right]$	Ordinary diffusion force
$D_{ij}$	$\frac{n_i n_j}{n} \frac{r_i + r_j}{K_{ij}} \left[ \frac{\pi(m_i + m_j) T_D}{32 m_i m_j} \right]^{1/2}$	Local diffusion coefficient between two species $i$ and $j$
$K_{ij}$	$\left( \frac{\pi}{3} \right) g_{ij} r_{ij}^3 n_i n_j (1 + e)$	Coefficient concerning the frequency of interaction
$g_{ij}$	$\frac{1}{(1-f)} + 6 \left( \frac{r_i r_k}{r_i + r_k} \right) \times \frac{\xi}{(1-f)^2} + 8 \left( \frac{r_i r_k}{r_i + r_k} \right)^2 \times \frac{\xi^2}{(1-f)^3}$	Radial distribution function
$\xi$	$2\pi(n_i r_i^2 + n_j r_j^2)/3$	area scale

646 divide the chute into equal sized bins in the  $y$ -direction of width  $\Delta y = 2$  mm. We calculate  
 647 stresses such considering the contribution from the part of each particle  $j$  within a bin of  
 648 width  $\Delta y$  centered at  $y$ .

649 We calculate the kinetic stress  $\sigma_{yy,n}^{\mathbf{k}}(y) = \rho_n v'_n v'_n(y)$  (the  $y$ -component of the normal

kinetic stress of species  $n$ ) using a relatively standard procedure (as in Ref. [29]):

$$\sigma_{yy,n}^{\mathbf{k}}(y) = \frac{\rho_{m,n}}{N^2} \left( \sum_{i=1}^N \frac{\Sigma_j V_{ij,n}}{V_{bin}} \right) \left( \sum_{i=1}^N \frac{\Sigma_j [v_{ij,n} - v(y)]^2 V_{ij,n}}{\Sigma_j V_{ij,n}} \right). \quad (\text{B1})$$

Here,  $i$  refers to the  $i$ th time step of which there are  $N$ , and  $j$  refers to the  $j$ th particle (of species  $n$ ) that is partly or fully in this bin (at time step  $i$ ).  $V_{ij}^n$  and  $v_{ij}^n$  are the volume and velocity of that particle, respectively.  $V_{bin} = DL\Delta y$  is the total volume of the bin.  $v(y) = \Sigma_n [f^n(y)v^n(y)] / \Sigma_n f^n(y)$  is mean velocity at  $y$ . As in Section IV B,  $\sigma_{yy}^{\mathbf{k}}(y) = \Sigma_n \sigma_{yy,n}^{\mathbf{k}}(y)$ .

To calculate the local contact stress at each position  $y$ , we consider each interparticle contact  $K$  in a bin of width  $\Delta y$  centered at  $y$ . Then, we sum the stresses associated with each interparticle contact in each region, as in Refs. [55, 56]. Specifically, for the mixture in the  $y$ -direction, we calculate:

$$\sigma_{yy}^{\mathbf{c}}(y) = \frac{\sum_{\tau=1}^N \sum_{K=1}^{N_c(y)} F_{ijK,y} \cdot l_{ijK,y}}{NV_{bin}}. \quad (\text{B2})$$

Here,  $\mathbf{F}_{ijK,y}$  is the force of particle  $i$  on particle  $j$  associated with the  $K$ th contact in this bin, of which there are  $N_c(y, \tau)$  at time step  $\tau$ . There are  $N$  such timesteps.  $\mathbf{l}_{ijK,y}$  is the vector from the center of particle  $i$  to the center of particle  $j$ .

Since a contact may involve particles of different species, we consider three types of contacts separately in calculating the species contact stresses. (1) Contacts between two less dense particles only contribute to the partial contact stress of the less dense particles,

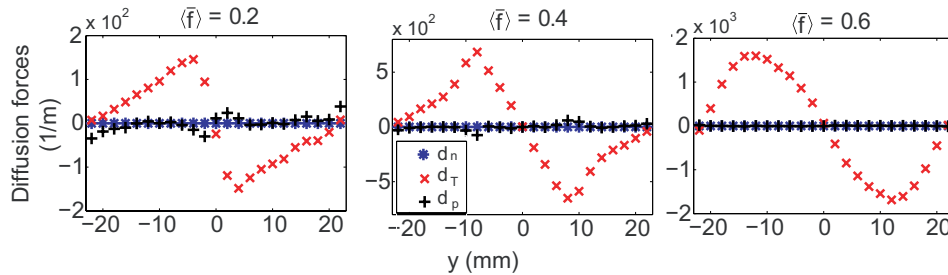


FIG. 12. (Color online) Profiles of driving forces in the  $y$ -direction averaged across the width of the chute and over the first 1 s for three  $\langle f \rangle$ 's as indicated in the figure. The three different diffusion forces are:  $d_T$ ,  $d_p$ , and  $d_n$  vs.  $y$ .



and we denote the stress associated  $K$ th such contact as  $\sigma_{K,ll}^c$ . (2) Contacts between two denser particles only contribute to the partial contact stress of the denser particles, and we denote the stress associated  $K$ th such contact as  $\sigma_{K,dd}^c$ . (3) Contacts between one less dense particle and one denser particles contribute to the contact stress of both species; we denote the stress associated  $K$ th such contact as  $\sigma_{K,ld}^c$ . As the size of two species is the same, for each collision between a less dense and denser particle, we divided the contribution of stress to the partial stresses equally between the two species. Based on that, we calculate the partial contact stress at  $y$  for particles of species  $n$  at time step  $\tau$  as:

$$\sigma_n^c(y, \tau) = \sum_{K=1}^{N_{c,n}(y)} \sigma_{K,nn}^c + \sum_{K=1}^{N_{c,j}(y)} \sigma_{K,nj}^c/2. \quad (\text{B3})$$

In this equation,  $\sigma_{K,nn}^c$  denotes the contact stress associated  $K$ th contact between a particle of type  $n$  with another particle of the same species in a bin of width  $\Delta y$  centered at  $y$ , of which there are  $N_c^i(y)$ .  $\sigma_{K,nj}^c$  denotes the contact stress associated  $K$ th contact between two particles of different species in a bin of width  $\Delta y$  centered at  $y$ , of which there are  $N_c^j(y)$ . We calculate the average stress over  $N$  time steps:

$$\sigma_n^c(y) = \sum_{\tau=1}^N \sigma_n^c(y, \tau)/N. \quad (\text{B4})$$

We note that this satisfies  $\sigma^c(y) = \sigma_l^c(y) + \sigma_d^c(y)$ , as specified in Section IV B.

- 
- [1] C. Tai, S. Hsiau, and C. Krueger, Powder Technology **204**, 255 (2010).  
[2] E. W. C. Lim, AIChE Journal **56**, 2588 (2010).  
[3] C. Zeilstra, M. A. van der Hoef, and J. A. M. Kuipers, Phys. Rev. E **77**, 031309 (2008).  
[4] N. Shishodia and C. R. Wassgren, Phys. Rev. Lett. **87**, 084302 (2001).  
[5] J. Saxton, P. Fralick, U. Panu, and K. Wallace, Economic Geology **103**, 1657 (2008).  
[6] O. Frihy and P. Komar, Marine Geology **115**, 253 (1993).  
[7] R. Slingerland, Marine Geology **47**, 753 (1977).  
[8] E. Viparelli, L. Solari, and K. M. Hill, Sedimentology, Accepted (2015).  
[9] N. Burtally, P. J. King, and M. R. Swift, Science **295**, 1877 (2002).  
[10] D. V. Khakhar, J. J. McCarthy, and J. M. Ottino, Phys. Fluids **9**, 3600 (1997).  
[11] K. M. Hill, D. V. Khakhar, J. F. Gilchrist, J. J. McCarthy, and J. M. Ottino, Proc. Nat. Acad. Sci. **96**, 11701 (1999).

- [12] N. Jain, J. M. Ottino, and R. M. Lueptow, Phys. Rev. E **71**, 051301 (2005).
- [13] S. Sarkar and D. V. Khakhar, Europhys. Lett. **83**, 54004 (2008).
- [14] L. Sanfratello and E. Fukushima, Granular Matter **11**, 73 (2009).
- [15] G. C. Pereira, M. D. Sinnott, P. W. Cleary, K. Liffman, G. Metcalfe, and L. D. Sutalo, Granular Matter **13**, 53 (2011).
- [16] N. K. Mitani, H. G. Matuttis, and T. Kadono, Geophysical Research Letters **31**, L15606 (2004).
- [17] K. M. Hill and Y. Fan, Phys. Rev. Lett. **101**, 088001 (2008).
- [18] J. T. Jenkins and D. K. Yoon, Phys. Rev. Lett. **88**, 194301 (2002).
- [19] Y. Fan, *Shear-induced segregation in dense granular mixtures.*, Ph.D. thesis, University of Minnesota (2011).
- [20] J. E. Galvin, S. R. Dahl, and C. M. Hrenya, J. Fluid Mech. **528**, 207 (2005).
- [21] S. L. Conway, X. Liu, and B. J. Glasser, Chemical Engineering Science **61**, 6404 (2006).
- [22] J. T. Jenkins and F. Mancini, Phys. Fluids A **1**, 2050 (1989).
- [23] D. K. Yoon and J. T. Jenkins, Phys. Fluids **18**, 073303 (2006).
- [24] M. Louge and J. Jenkins, in *Mechanics of deformation and flow of particulate materials* (ASCE, 1997) pp. 370–379.
- [25] H. Xu, M. Louge, and A. Reeves, Continuum Mech. Thermodyn. **15**, 321 (2003).
- [26] Y. Fan and K. M. Hill, Phys. Rev. Lett. **106**, 218301 (2011).
- [27] A. Tripathi and D. V. Khakhar, Phys. Rev. Lett. **107** (2011).
- [28] A. Tripathi and D. V. Khakhar, Journal of Fluid Mechanics **717**, 643 (2013).
- [29] Y. Fan and K. M. Hill, New J. Phys. **13**, 095009 (2011).
- [30] Y. Fan and K. M. Hill, Phys. Rev. E **81**, 041303 (2010).
- [31] P. A. Cundall and O. D. L. Strack, Geotechnique **29**, 47 (1979).
- [32] R. D. Mindlin and H. Deresiewicz, J. Appl. Mech. Trans. ASME **20**, 327 (1953).
- [33] Y. Tsuji, T. Tanaka, and T. Ishida, Powder Technol. **71**, 239 (1992).
- [34] O. Pouliquen and R. Gutfraind, Phys. Rev. E **53**, 552 (1996).
- [35] GDRMiDi, Eur. Phys. J. E **14**, 341 (2004).
- [36] V. Chikkadi and M. Alam, Phys. Rev. E **80**, 021303 (2009).
- [37] K. M. Hill and J. Zhang, Phys. Rev. E **77**, 061303 (2008).
- [38] J. Choi, A. Kudrolli, R. Rosales, and M. Bazant, Phys. Rev. Lett. **92**, 174301 (2004).

- 722 [39] R. D. Wildman and D. J. Parker, Phys. Rev. Lett. **88**, 064301 (2002).
- 723 [40] K. Feitosa and N. Menon, Phys. Rev. Lett. **88**, 198301 (2002).
- 724 [41] E. D. Liss, S. L. Conway, and B. J. Glasser, Phys. Fluids **14**, 3309 (2002).
- 725 [42] K. Hill and D. S. Tan, J. Fluid Mech. **756**, 54 (2014).
- 726 [43] G. K. Batchelor, *An Introduction to Fluid Dynamics* (Cambridge University Press, Cambridge,  
727 UK, 2000).
- 728 [44] H. Schlichting, *Boundary-Layer Theory* (McGraw-Hill, New York, 1979).
- 729 [45] L. W. Morland, J. Geophysical Research **77**, 890 (1972).
- 730 [46] L. W. Morland, Geophys. J. R. Astron. Soc. **55**, 393 (1978).
- 731 [47] L. W. Morland, Surv. Geophys. **13**, 209 (1992).
- 732 [48] J. M. N. T. Gray and A. R. Thornton, Proc. R. Soc. A **461**, 1447 (2005).
- 733 [49] J. M. N. T. Gray and V. A. Chugunov, J. Fluid Mech. **569**, 365 (2006).
- 734 [50] Y. Fan, C. P. Schlick, P. B. Umbanhowar, J. M. Ottino, and R. M. Lueptow,  
735 J. Fluid Mech. **741**, 252 (2014).
- 736 [51] M. Larcher and J. Jenkins, Physics of Fluids **25**, 113301 (2013).
- 737 [52] G. Félix and N. Thomas, Phys. Rev. E **70**, 051307 (2004).
- 738 [53] J. Zhang and K. M. Hill, (2011), under review.
- 739 [54] K. M. Hill, Y. Fan, J. Zhang, C. Van Niekerk, E. Zastrow, S. C. Hagness, and J. T. Bernhard,  
740 Granular Matter **12**, 201 (2010).
- 741 [55] C. S. Campbell, J. Fluid Mech. **465**, 261 (2002).
- 742 [56] E. Kuhl, G. A. D’Addetta, H. J. Herrmann, and E. Ramm, Granular Matter **2**, 113 (2000).